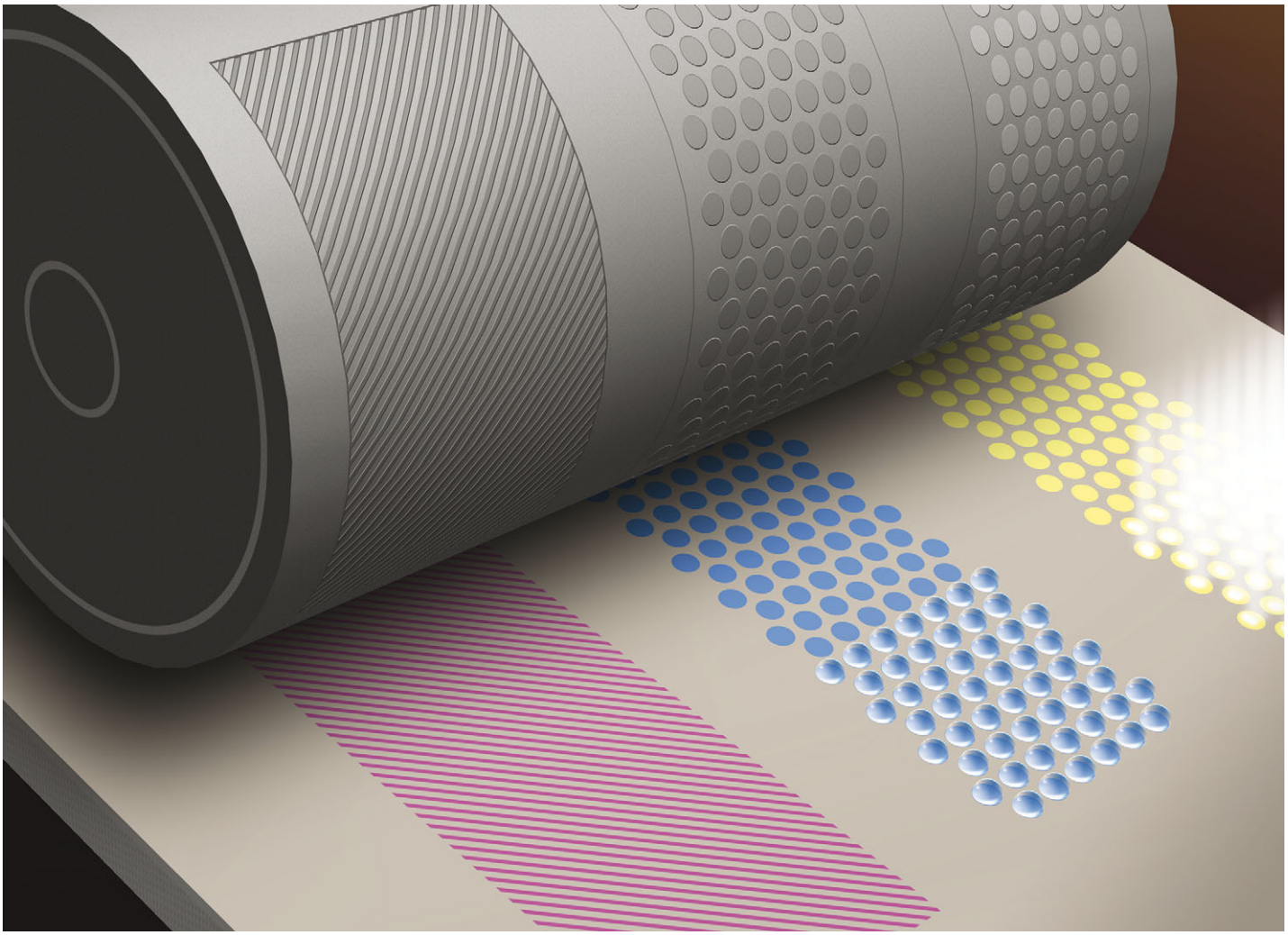

Showcasing research from Hajim School of Engineering & Applied Sciences, Department of Chemical Engineering, University of Rochester.

Urethane–acrylate polymers in high-resolution contact printing

Polyurethane–acrylates are used in contact printing applications to pattern organic molecules and thin films with high resolution and uniformity. Printed thin films of organic semiconductors with sub-micrometer lateral dimensions and sub-100 nm thicknesses are used to manufacture OLED devices.

As featured in:

See Alexander A. Shestopalov *et al.*, *J. Mater. Chem. C*, 2016, **4**, 4155.

ROYAL SOCIETY OF CHEMISTRY

www.rsc.org/MaterialsC

Registered charity number: 207890

Journal of
Materials Chemistry C

PAPER

Cite this: J. Mater. Chem. C, 2016, 4, 4155

Urethane–acrylate polymers in high-resolution contact printing†

Jinhai Li, Lisong Xu, Soyoun Kim and Alexander A. Shestopalov*

Received 17th March 2016,
Accepted 14th April 2016

DOI: 10.1039/c6tc01125j

www.rsc.org/MaterialsC

This study describes polyurethane–acrylates (PUAs) as polymeric stamp materials that can be used in a number of contact printing applications. We demonstrate that the surface energy of PUA polymers can be controlled chemically, producing stamps with tunable polarity and eliminating the need to apply release coatings or to adjust stamping kinetics to facilitate material transfer. To demonstrate the general nature of the proposed materials, PUA polymers were used in the contact printing of organic molecules and organic thin films. The results suggest that PUA-based contact printing can be used as a simple alternative to a kinetically modulated PDMS stamping of thin films, and that thin film features with sub-micrometer lateral dimensions and sub-100 nm thicknesses can be accurately reproduced using a universal set of printing conditions.

Introduction

The concept of patterning micro- and nano-structures *via* simple contact printing offers an attractive manufacturing platform that does not rely on expensive vacuum or photo-based pattern replication. Because of this potential, the ability to transport and align thin layers of organic and inorganic materials to large-area substrates with nanoscopic precision and uniformity has become a long-standing desire of engineers and scientists in the field of contact printing.

Since 1993, after Whitesides and co-workers have proposed a contact printing technique to form patterned self-assembled monolayers (SAMs) of alkylthiols on gold using elastic polydimethylsiloxane (PDMS) stamps,[1] the field of soft-lithographic contact printing has attracted significant interest. Multiple methods for patterning organic and biological monolayers using polymeric stamps have been reported.[2–14] In parallel, significant progress has been made with the exploration of contact printing in thin film patterning[15–20] and colloidal printing and assembly.[21,22] In these methods a functional film is either directly deposited on the patterned elastomeric stamp or picked up from the donor surface by the stamp and then transferred to the receiver substrate *via* conformal stamp–substrate contact to form a pattern of features identical to the pattern on the stamp. This process relies on the delamination and association of materials at the stamp–ink–substrate interfaces, and it is primarily governed by interfacial adhesion – a function of material elasticity, surface energy, stamping direction and printing kinetics.

Since the discovery of soft-lithographic printing, the majority of the reported contact printing methods have relied on the hydrophobic PDMS material to form patterned stamps. However, the elasticity and surface energy of PDMS cannot be easily modified without sacrificing its mechanical stability. Therefore, stamping conditions in PDMS-based printing has been traditionally optimized around its constant physical properties. For example, in small molecule and biomolecule transfer, hydrophobic PDMS stamps are often treated with oxygen plasma to make them wettable with polar materials. Such treatment only temporarily changes PDMS polarity, alters feature dimensions, and often results in surface cracking.[23–25] In thin film printing, the delamination and deposition processes of PDMS stamps have to be modulated by the stamping kinetics only,[18] because they cannot be directly controlled by changing PDMS surface energy. The viscoelastic properties of PDMS also limit the size of thin film features that can be replicated with contact printing. Some reports show that the Young's modulus of PDMS is too low to accurately replicate sub-100 nm features,[26,27] and that the modulation of material transfer with the stamping kinetic is only possible with features larger than ~1 micrometer.[18,28] Moreover, PDMS stamps can accurately transfer patterns only from the features with 0.2–2 aspect ratios,[26,29–31] complicating the use of PDMS in the replication of complex patterns containing a combination of large and small objects.

Some of the mentioned limitations of PDMS-based printing can be avoided by replacing PDMS with another polymer. For example, a commercially available polyurethane–acrylate (PUA)[32–34] mixture has been used in several micro- and nano-contact printing techniques. PUA has higher surface energy than PDMS

Department of Chemical Engineering, University of Rochester, Rochester, New York 14627, USA. E-mail: alexander.shestopalov@rochester.edu

† Electronic supplementary information (ESI) available: Experimental details and characterization methods. See DOI: 10.1039/c6tc01125j

(PUA 48 mN m^{-1} *vs.* PDMS 21 mN m^{-1}) permitting inking with hydrophilic materials. Yoo *et al.* demonstrated that PUA can be successfully applied in the traditional microcontact printing of organic molecules.[35] PUA is more rigid than PDMS (E_{PUA} ~ 10 MPa *vs.* E_{PDMS} 1–3 MPa), yet flexible enough to spontaneously adhere to interfaces, permitting the accurate replication of small sub-100 nm features and complex patterns with significant feature aspect ratio variations. We demonstrated that chemically modified PUA stamps bearing sub-100 nm features with 0.04 aspect ratios can be used in catalytic soft lithography to accurately reproduce chemical patterns on gold and silicon with sub-40 nm edge resolution.[36–40]

PUA has also been applied in thin film transfer. Kwak *et al.* demonstrated that 20–200 nm thick Al and Au thin films can be printed from PUA stamps.[41] The authors demonstrated that PUA is rigid enough to accurately replicate 70 nm lines; however, a thin poly(ethylene terephthalate) (PET) layer was required between PUA and the metal film to enable the transfer. Choi *et al.* demonstrated that spincoated polymeric films of PMMA and P3HT can be transferred from PUA to silicon and flexible polycarbonate supports *via* contact printing with reasonable feature uniformity and 70 nm resolution.[42] Several groups also demonstrated the replication of thin organic films with nanoscopic precision using PUA polymers as printing stamps.[43–47] However, the use of PUA in these methods has been often complicated by the necessity to control its surface energy with thin adhesive/release layers that are applied to the PUA surface before printing.[41,43,45,46] Such processing complicates the procedure and can contaminate the deposited films.

In this article, we describe several polyurethane–acrylate (PUA) polymers that can be used as PDMS replacement in contact printing techniques. We demonstrate that the surface energy of PUA polymers can be controlled chemically, producing stamps with tunable polarity and eliminating the need to apply adhesive or release coatings to facilitate material transfer. To demonstrate the general nature of the proposed materials, we used PUA polymers in the contact printing of hydrophobic and hydrophilic organic molecules and organic thin films.

Results and discussion

Urethane–acrylate polymers

To tune the surface energy of the elastic stamps and to use them in contact printing, we required a polymer that is sufficiently elastic to uniformly conform to large-area substrates, sufficiently rigid to avoid the collapse and deformation of features, and amenable to polymerization with different hydrophobic/hydrophilic monomers. Acrylate-based polymers have been previously used in soft lithography.[48] Their prepolymeric mixtures can be functionalized through the covalent attachment of primary amines or thiols *via* Michael addition. However, a significant limitation to the use of acrylamide stamps was reported previously:[49] while these materials are easily functionalized, they lack the mechanical rigidity necessary for high fidelity transfer at short length scales. Polyurethane–acrylate mixtures with an ~10 MPa modulus avoid this limitation. For example, they were previously used to prepare stamps with densely arrayed nanopatterns of sub-100 nm features with high aspect ratios for use in replica molding. PUA mixtures produce highly accurate defect-free stamps with densely arrayed features that do not collapse laterally.[32,33,50] At the same time, similar to traditional acrylates, PUA can be easily modified with various nucleophilies *via* Michael addition to change the bulk and surface properties of the resulting polymerized stamps. In this work, we used the previously reported PUA mixture[37] as a starting material for polymers with tunable surface energies.

The PUA monomer (**1**) was prepared from isophorone diisocyanate, polyethylene glycol (av. M_W 400 g mol^{-1}), and hydroxypropyl acrylate following a previously published protocol.[39] Monomer **1** was then diluted by 30% with trimethylolpropane ethoxylate triacrylate **2** (av. M_W 912 g mol^{-1}) to reduce viscosity and to provide additional functionalization points (Fig. 1). This mixture was diluted with small amounts of photoinitiators and polymerized under UV light between transparent glass slides to produce an unfunctionalized polyurethane–acrylate (**PUA**) polymer. In addition, prior to polymerization, the mixture of **1** and **2** was reacted *via* Michael addition with polyethylene glycol mercaptane (**PEG-SH**) or with perfluorinated primary alkyl amine (**F-NH_2**) to produce PUA polymers **PEG-PUA** and **F-PUA** modified with hydrophilic polyethylene glycol or hydrophobic perfluorinated units (Fig. 1).

Prepared flat polymers were analyzed by goniometry and mechanical deformation to determine their surface energies and Young's moduli (Fig. 1). As expected, the addition of the hydrophilic **PEG-SH** increased the surface energy of **PEG-PUA** (53 mN m^{-1}, ~4.8 v/v% of **PEG-SH**), while the hydrophobic **F-NH_2** decreased the surface energy of **F-PUA** to 23 mN m^{-1}. These values

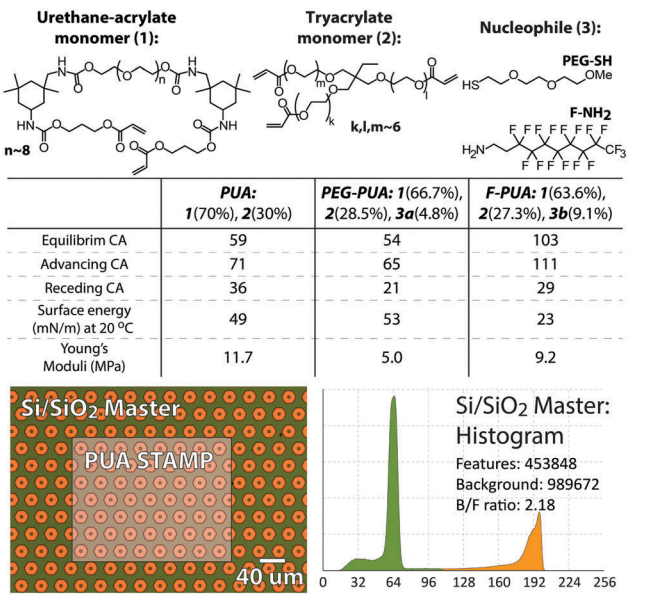

	PUA: ***1***(70%), ***2***(30%)	*PEG-PUA:* ***1***(66.7%), ***2***(28.5%), ***3a***(4.8%)	*F-PUA:* ***1***(63.6%), ***2***(27.3%), ***3b***(9.1%)
Equilibrim CA	59	54	103
Advancing CA	71	65	111
Receding CA	36	21	29
Surface energy (mN/m) at 20 °C	49	53	23
Young's Moduli (MPa)	11.7	5.0	9.2

Fig. 1 Top scheme: PUA components; middle table: contact angles (CA), surface energy and Young's modulus of PUA polymers; bottom micrograph and histogram: overlapped micrographs of the patterned master and stamp, and a histogram of the master image showing the ratio of the background to featured areas.

This journal is © The Royal Society of Chemistry 2016

cover the range of surface energies of the majority of common polymeric materials (from Teflon™ to polyamides), suggesting that the described polymeric system and functionalization approach can be used to prepare materials with diverse adhesive and wetting properties. The Young's moduli of the prepared polymers decrease with the addition of **PEG-SH** and **F-NH$_2$** nucleophiles, probably due to the lower degree of crosslinking in the functionalized **PEG-PUA** and **F-PUA** due to the reaction of the acrylate ends with mono-substituted amines and thiols. The Young's modulus of the **PEG-PUA** decreased more than that of **F-PUA**, probably due to the lower entropy of the **F-PUA** network that contains dissimilar (–C$_X$F$_Y$) and (–CH$_2$–CH$_2$–O–) fragments.

Patterned PUA stamps were prepared by polymerizing the corresponding pre-polymeric mixtures between a glass slide and a silicon/silicon oxide master under UV light for 4 hours at room temperature. Our previous AFM and SEM measurements demonstrate that these conditions lead to accurate replication of the master features with the correct aspect ratio values.[38,39] Following polymerization, the stamps were peeled off from the master, rinsed with isopropanol and water and stored under ambient conditions in a dust-free environment. We used several different masters containing arrays of microscopic features. The size and the fidelity of the features on the stamps and on the silicon masters were identical to each other: Fig. 1 demonstrates that superimposed images of the patterned stamp and the master overlap completely without noticeable defects. The stamp features were reproduced uniformly throughout the entire area of the PUA stamp ($\sim 3 \times 3$ cm^2). Previously, it was reported that polyurethane–acrylate stamps are chemically inert and do not degrade in organic solvents or at temperatures below 150 °C.[38,39] Our observations are in agreement with these reports. The dimensions of the features on the prepared **PUA**, **PEG-PUA** and **F-PUA** stamps did not change over time or after exposure to water and organic solvents (30 minute exposure at 23 °C to ethanol, isopropanol, toluene, hexane, and dimethylformamide).

Dynamic mechanical analysis (DMA) was performed to examine viscoelastic behavior of the prepared polymers. Fig. 2 demonstrates that the storage moduli of PUA polymers decrease with temperature and reach a minimum rubbery plateau at ~40–50 °C. The non-functionalized **PUA** polymer that demonstrated a higher storage modulus at all tested temperatures then modified **PEG-PUA** and **F-PUA** due to the higher degree of cross-linking. Fig. 2 also shows that prepared polymers have glass transition temperatures below 20 °C. DMA analysis suggests that the optimal printing temperature for the prepared PUA polymers should be higher than 40 °C (higher than 30 °C for the **PEG-PUA**) when the storage modulus is low, to facilitate uniform and conformal stamp–substrate adhesion without a significant applied force.

We also examined the dependence of the adhesion of the unmodified **PUA** stamp on the applied pressure and temperature. In these experiments, the patterned **PUA** stamp (1 cm^2 total stamp area, 44 : 46% feature to background ratio) was analyzed on a uniaxial electromechanical load frame to determine how the vertical separation pull-off force of the patterned stamp depends on the initial applied pressure and temperature.

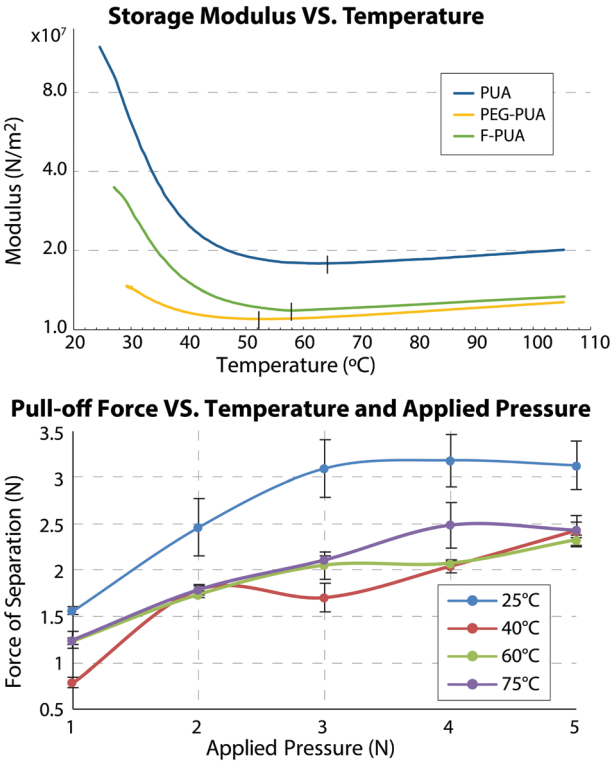

Fig. 2 Top: Dynamic mechanical analysis of polyurethane–acrylate polymers; bottom: vertical pull-off force *vs.* applied pressure and temperature of the patterned PUA.

In these experiments, the stamp was mounted on the force cell, heated to the desired temperature and brought into contact with a clean silicon substrate at the desired pressure. Subsequently, a force–displacement curve was collected for each experiment to determine the separation force and the stamp expansion. Fig. 2 shows the dependence of the average separation force (from 10 displacement experiments for each T, P point) as a function of the initial contact load and temperature. It demonstrates that the pull-off force decreases as the temperature increases from 25 °C to 40 °C, and that it remains largely constant in the 40–75 °C region. We assume that the initial decrease of the pull-off force with temperature is associated with the transition of the polymer from a semi-glassy to a rubbery state at 35–45 °C (Fig. 2 top, blue line for the **PUA** stamp). This suggests that the pull-off force is proportional to the polymer storage modulus and that it is constant at the rubbery plateau temperatures. Fig. 2 also suggests that there is a minimal applied force that must be attained to achieve the highest possible adhesion, and that the further increase in the applied pressure does not change the force of adhesion. The data in Fig. 2 suggest that the optimal printing temperature for the PUA polymers should be higher than 50 °C when they completely transit into the low adhesion, rubbery regime, and that the increase in the **PUA** storage modulus leads to the stronger adhesion.

To demonstrate that PUA stamps can be used in the contact patterning of a variety of materials, we used them in the transfer printing of traditional organic SAMs and organic thin films.

We used sputtered indium tin oxide (ITO) as a receiver substrate for the majority of our experiments. ITO is a popular electrode in organic electronic devices, due to its electrical conductivity and optical transparency.[51,52] It is used routinely in the fabrication of liquid crystal displays (LCDs), organic light emitting diodes, and organic photovoltaic devices.[53–57] Considering that the majority of ITO-based devices require the lateral patterning of its components, a family of polymers that can structure various components of practical electronic devices on ITO will be of interest to a broad community of materials scientists.

Molecular ink transfer

Previously, commercially available PUA polymers had been used in the traditional microcontact printing of hydrophobic thiols on gold.[35] To demonstrate that the prepared polymers can pattern hydrophilic and hydrophobic organic molecules on ITO, we used them in the microcontact printing of fluorinated and PEG-modified phosphonic acids. The goal of these experiments was to demonstrate that unlike the majority of PDMS-based techniques, microcontact printing with PUA stamps can directly pattern both hydrophobic and hydrophilic SAMs.

SAMs are typically formed on ITO using organosilanes, carboxylic acids, phophonic acids or thiols.[58–66] Neither carboxylic acids nor thiols bind strongly to ITO, and monolayers of these species are labile.[67] Organosilanes and phosphonic acids, however, have been shown to bind strongly to ITO, forming homogenous, oriented monolayers.[68–70] Trichloro- and trialkoxysilanes, however, react slowly with ITO and require dry or inert conditions to avoid polymerizations. Reactions of ITO with trichlorosilanes also produce HCl that slowly etches ITO. Therefore, in this work, we took advantage of the stability, order and fast reactivity imparted by phosphonic acids to create patterns of SAMs on ITO using PUA stamps. Patterned and flat **PUA**, **PEG-PUA** and **F-PUA** stamps were wetted with corresponding solutions (10 mmol) of aliphatic (**Alk-PA**), PEG-modified (**PEG-PA**) and fluorinated (**F-PA**) phosphonic acids in isopropanol (**PEG-PA** in methanol). The stamps were dried under the stream of filtered nitrogen and placed on clean ITO substrates. Small pressure was applied only initially to ensure conformal contact. Subsequently, the stamps were allowed to react with ITO for 1 min without external pressure at room temperature. After the printing, the stamps and the substrates were separated, rinsed with isopropanol and dried with filtered nitrogen.

Fig. 3 shows the SEM images of the patterned monolayers of **F-PA**, **Alk-PA** and **PEG-PA** molecules printed using different polyurethane–acrylate stamps (**F-PUA**, **PUA** and **PEG-PUA**). The contrast in the SEM images of the printed SAMs is due to the differences in the intensities of the secondary electrons emitted from the clean ITO and ITO modified with organic monolayers. The printed features show a uniform grayscale intensity suggesting that the density of the printed SAMs is uniform within the individual features and over the entire pattern. The features were reproduced without noticeable defects and they were present on the entire substrate area (measured in at least three different areas). The ratios of the background areas to the areas occupied by the printed features were calculated from the greyscale

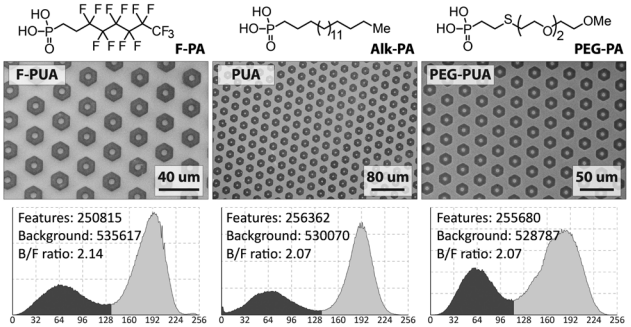

Fig. 3 Top structures: molecular structures of the printed self-assembled monolayers; middle images: SEM images of the monolayers printed using corresponding PUA stamps; bottom histograms: grayscale histograms and background-to-feature ratios of the printed SAMs.

histograms of the original SEM images (Fig. 3, bottom). The background-to-feature ratios of the **F-PA**, **Alk-PA** and **PEG-PA** SAMs were similar to each other (2.14 : 2.07 : 2.07) and to the background-to-feature ratio of the silicon master, calculated from the RGB histogram of the master optical micrograph (2.18; Fig. 1, bottom). These calculations suggest that perfluorinated **F-PUA**, unmodified **PUA**, and PEG-modified **PEG-PUA** stamps can replicate SAMs of hydrophobic **F-PA**, aliphatic **Alk-PA** and hydrophilic **PEG-PA** molecules in traditional diffusive microcontact printing without noticeable defects and preserving the original feature shapes and dimensions.

The quality of the printed SAMs was assessed by comparing the monolayers of phosphonic acids printed with flat PUA stamps to the analogous SAMs deposited overnight at room temperature from 10 mmol isopropanol solutions (methanol solution for **PEG-PA**). Contact angle goniometry measurements demonstrate that the surface energies and water contact angles of the printed and solution deposited monolayers match each other (Fig. 4). The contact angle hysteresis – the difference between the advancing and receding contact angles – was higher for all printed SAMs, suggesting that they have less ordered structure than the solution-deposited monolayers. X-ray photoelectron spectroscopy (XPS) analysis revealed that the characteristic atomic peaks of the printed and solution deposited monolayers (F 1s in **F-PA**, and C 1s in **Alk-PA** and **PEG-PA**) have identical shapes and the same electron-state components (Fig. 4). For example, F 1s scans of the printed and solution deposited **F-PA** SAMs contain both CF_3– and –CF_2– components separated by 4 eV; **Alk-PA** SAMs demonstrate a single C 1s peak at 284.5 eV that corresponds to the aliphatic C–C bonds, while C 1s scans of **PEG-PA** SAMs show two fused peaks at 285.5 and 284 eV from the C–O and C–C bonds (Fig. 4, middle).

We also demonstrated that the printed SAMs of **Alk-PA** molecules are dense and ordered enough to serve as etch resists against a 50 mmol oxalic acid aqueous solution that dissolves ITO at 12 nm s^{-1} rate under ambient conditions.[71] As such, ITO substrates containing two different patterns of the **Alk-PA** SAMs printed using **PUA** stamps were submerged in 50 mmol oxalic acid solution for 30 s. Subsequently, the substrates were rinsed with water and isopropanol, and imaged using circular differential

 This journal is © The Royal Society of Chemistry 2016

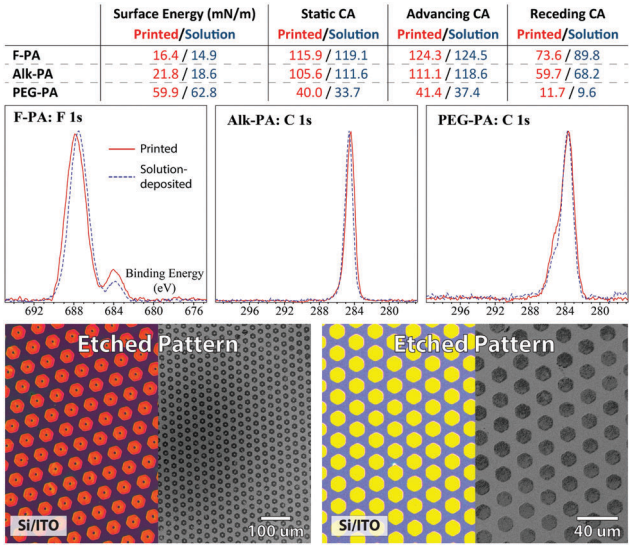

Fig. 4 Top table: surface energy and water contact angle measurements of the printed and solution-deposited monolayers of **F-PA**, **Alk-PA** and **PEG-PA** phosphonic acids, middle spectra: superimposed F 1s and C 1s XPS spectra of the printed and solution-deposited monolayers; bottom micrographs: C-DIC micrographs (color) and SEM images (grayscale) of the patterned ITO formed by etching printed SAMs of **Alk-PA** with 50 mmol oxalic acid aqueous solution. Micrographs show two different patterns, one of which contains hexagonal rings with ~1 μm inside holes.

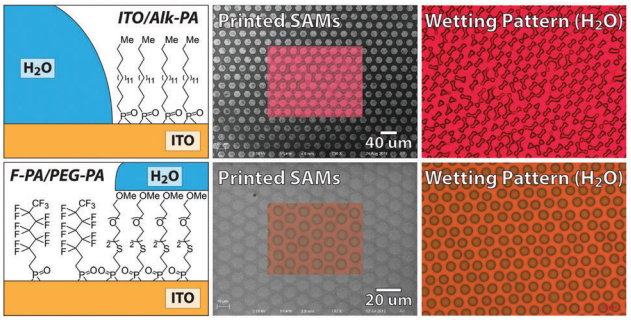

Fig. 5 Top row: amphiphilic pattern of hydrophobic **Alk-PA** SAMs on oxidized ITO. SEM and optical images of the printed SAMs and water droplets. The SEM inset shows a superimposed overlay of the SAM and water patterns. Bottom row: amphiphilic pattern of hydrophilic **PEG-PA** SAMs on **F-PA** covered ITO. SEM and optical images of the printed SAMs and water droplets.

interference contrast (C-DIC) microscopy and SEM. Fig. 4 shows physical features that were formed on ITO substrates after the etching. The C-DIC images of the etch patterns show clear contrast in colors confirming the existence of height differences between the features and the background. The etched patterns were replicated with good fidelity preserving even the small (~1 μm) inside holes in the hexagonal ring pattern, suggesting that the printed SAMs of **Alk-PA** molecules are dense enough to serve as molecular etch resists. These results confirm that PUA polymers can serve as suitable stamp materials in the traditional microcontact printing of dense hydrophobic and hydrophilic organic self-assembled monolayers.

To demonstrate the utility of patterning both hydrophilic and hydrophobic monolayers, we used PUA stamps to create amphiphilic patterns on ITO that can direct a two-dimensional liquid assembly. We first prepared substrates containing patterns of hydrophobic aliphatic phosphonic acids (**Alk-PA**) on oxidized ITO using traditional microcontact printing with the **PUA** stamp (Fig. 5, top), and substrates containing patterns of hydrophobic per-fluorinated phosphonic acids (**F-PA**) printed with the **F-PUA** stamp on top of the continuous hydrophilic SAM of **PEG-PA** (Fig. 5, bottom). Subsequently, both substrates were exposed to water vapors and imaged using optical microscopy. Fig. 5 demonstrates that on the **ITO/Alk-PA** substrate water droplets organize around printed features, forming a repeated pattern of narrow channels, which, when superimposed with the SEM image of the printed monolayers, duplicate the dimension and distribution of the unfunctionalized hydrophilic area of the oxidized ITO. The **F-PA/PEG-PA** sample demonstrates an inverse pattern, where the water droplets organize into an ordered pattern of dots positioned on top of the patterned **PEG-PA** SAMs. This distribution is mostly accurate with only a small portion of defect elements (pattern voids and merged droplets). The size of the water droplets was uniform throughout the sample (imaged in at least 3 different locations) and matched the dimensions of the printed **PEG-PA** features (Fig. 5, bottom). These experiments show that by combining different stamp materials and micro-patterning techniques, we can create functional micro-patterns for liquid-collection and assembly.

Organic thin film transfer

In thin film printing, the effective material transfer relies on the control of adhesion and fracture mechanics at the "substrate"–"thin film"–"stamp" interfaces. These parameters are primarily determined by the surface energy and interfacial thermodynamics; in addition, they can be controlled *via* contact kinetics. The majority of the reported thin film transfer methods relies on the hydrophobic PDMS stamps whose surface energy cannot be easily adjusted. As a result, thin film delamination/deposition in these techniques is primarily controlled by the rate-dependent effects of viscoelastic PDMS stamps.[72–76] Although such rate modulation is effective, it requires careful optimization and control of stamping velocity, force distribution and feature geometry for each new "substrate–thin film–stamp" system. Moreover, such rate-dependent adhesion was primarily used for printing large 50–100 μm features, and its adaptation to smaller meso-patterns (0.1–5 μm) has not been demonstrated.

In this study, we demonstrate that the thin film transfer from elastic stamps can be controlled by the surface energy of the elastomer, without relying on contact kinetics. We used PUA stamps to pattern the emitting layers of the organic light-emitting diodes (OLEDs). OLEDs were used because in addition to traditional SEM and AFM imaging, the printing efficiency of our method can be analyzed *via* fluorescence microscopy and device electroluminescence. For the device to function, all components of the multilayered OLEDs must remain in conformal molecular contact, and the temperature sensitive layers must not degrade during the patterning step. Thus, by examining device electroluminescence and emitting layer fluorescence,

we can determine if the printing produces uniform van der Waals contacts between the layers and if it causes material degradation.

We first examined the ability of PUA polymers to transfer thin films of tris(4-carbazoyl-9-ylphenyl)amine (TCTA) doped with bis[2-(4,6-difluorophenyl)pyridinato-C^2,N](picolinato)iridium(III) (Firpic, light-emitted layer) to evaporated thin films of 4,4′-cyclohexylidenebis[*N*,*N*-bis(4-methylphenyl)benzenamine] (TAPC, hole-transporting layer). Thin films of TCTA/Firpic (20 nm) were evaporated on **PUA** (γ = 48.8 mN m^{-1}), **PEG-PUA** (γ = 53 mN m^{-1}) and **F-PUA** (γ = 23 mN m^{-1}) stamps bearing patterns of 8 μm hexagons. Hole-transport layers of TAPC (30 nm) were evaporated on ITO/MoOx electrodes. The stamps were brought in conformal contact with the TAPC substrates and held in contact at various temperatures at 110 kPa pressure for 10 minutes. Considering that the typical stamping time in the rate-modulated printing is usually in milliseconds, we believe that the 10 minute printing time in our experiments ensures that the stamp adhesion is not affected by the stamping kinetics. Subsequently, the printed patterns were examined for accuracy and uniformity using fluorescence microscopy. Printing with the hydrophobic **F-PUA** stamps at 23–170 °C did not result in the material transfer from the stamp to the substrate. Stamps with higher surface energies – **PUA** and **PEG-PUA** – successfully transferred patterned TCTA/Firpic films on the TAPC modified substrates at 50–80 °C. We think that the difference in the film transfer between hydrophobic and hydrophilic stamps is due to the differences in the interfacial surface energies of the "stamp–TCTA" and "TCTA–TAPC" interfaces, and the differences in the interfacial conformity between the vapor-created and mechanically-induced contacts. Both TCTA and TAPC molecules are hydrophobic and have similar molecular structures. Thus, the interface between these two materials is stabilized by the small surface energy difference and by the specific and favorable π–π intermolecular interactions. In contrast, the interface between hydrophilic stamps and TCTA has a significant surface energy mismatch and is not stabilized by any specific intermolecular forces. As a result, hydrophilic PUA stamps can successfully release vacuum-deposited TCTA films when mechanical contact between the film and the substrate is created. In contrast, the hydrophobic PUA stamp has surface energy that is much closer to that of TCTA. As a result, the vacuum-deposited TCTA films on the hydrophobic PUA have more uniform and stable contact that cannot be easily disrupted by the mechanical contact between the TCTA and TAPC films.

Fig. 6 shows fluorescence patterns of TCTA/Firpic films printed with **PEG-PUA** and **PUA** stamps at different temperatures. We used monochromatic histograms of the fluorescence patterns to determine the uniformity of the printed features. The patterns of features with non-uniform material distribution (**PEG-PUA** 40 °C; **PUA** 50–70 °C) contain two discrete peaks of the fluorescence pixels (to the right from the blue peak of the background pixels). Fig. 6 shows that uniform thin films of TCTA/Firpic can be patterned on TCTA at 50 °C with the **PEG-PUA** stamp and at 80 °C with the **PUA** stamp – these patterns demonstrate single symmetrical peaks of the fluorescence features, suggesting the uniform distribution of the fluorescent material within individual features and over the entire patterned area (each substrate was imaged in at least three different locations). Printing at higher temperatures results in the material transfer only at the edges of the individual features (**PEG-PUA** 60 °C; **PUA** 90 °C). With both stamps, we did not observe any material transfer when printing was conducted at 23 °C.

We suggest that the material transfer with **PEG-PUA** and **PUA** stamps depends on the modulus of the polymer and on the surface energy mismatch between the stamp and the thin film. With both polymers, successful transfer is achieved only after a complete transition of the polymers to a rubbery state

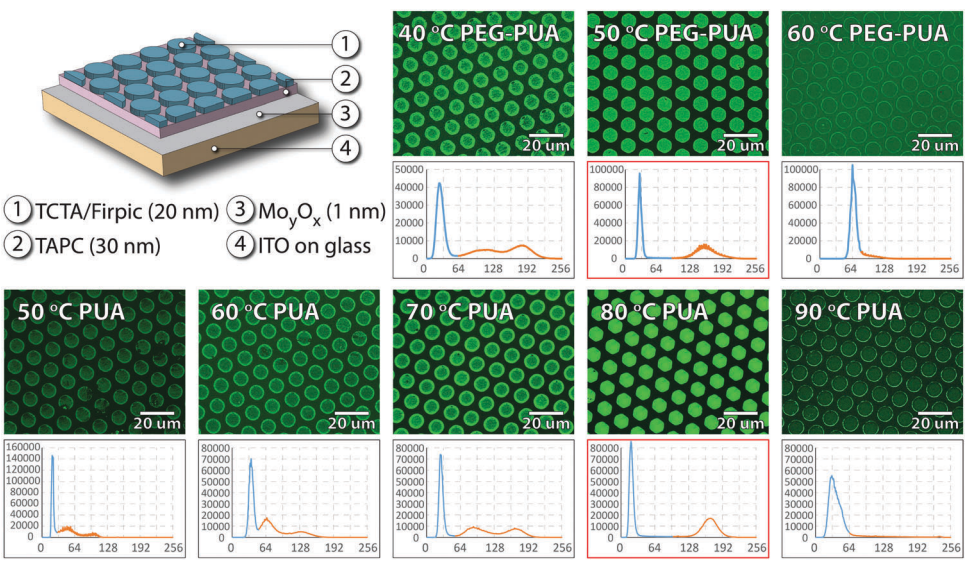

Fig. 6 Top left illustration: schematic illustration of the patterned TCTA/Firpic on TAPC-covered ITO; top right micrographs and histograms: fluorescence images of TCTA/FIrpic films printed with **PEG-PUA** at different temperatures and the corresponding monochromatic histograms of the fluorescence patterns; bottom micrographs and histograms: fluorescence images of TCTA/Firpic films printed with PUA at different temperatures and the corresponding monochromatic histograms of the fluorescence patterns.

This journal is © The Royal Society of Chemistry 2016

(**PEG-PUA:** 52 °C, **PUA:** 65 °C, Fig. 2 top). Pull-off force measurements of the **PUA** stamp also show that the adhesive force of the patterned stamp decreases and remains constant when the polymer undergoes complete transition into the rubbery plateau (Fig. 2 bottom). In addition, a slightly higher or lower energy of the PUA stamp creates stronger adhesion to the hydrophobic TCTA/Firpic layer, probably requiring higher temperature to enable complete separation. The reasons why both polymers failed to transfer TCTA/Firpic patterns at higher temperatures are unclear. We hypothesize that as the loss modulus of both polymers decreases with temperature, their Young's modulus eventually decreases to the point when the printing pressure causes feature deformations leading to non-conformal stamp–substrate contacts and preferential material transfer at the pattern edges.

Subsequently, we used XPS and optical microscopy to examine the accuracy and efficiency of our PUA printing. Fig. 7 shows the optical images and monochromatic histograms of the original silicon master and the fluorescence pattern. These images demonstrate that the feature/background ratios of both patterns are close to each other, suggesting that contact printing results in accurate feature replication and does not lead to the distortion of the feature geometries (images were taken in at least three different locations). To demonstrate that PUA printing results in complete material transfer, we analyzed printed substrates and stamps by XPS. As such, TAPC substrates with printed TCTA/Firpic features and the corresponding stamps were examined after the printing to determine Ir 4f and F 1s distribution between the stamps and the printed substrates. Both Ir and F atoms are present only in the Firpic molecule, making it possible to determine how this material is distributed between two interfaces by monitoring XPS signals of Ir 4d and F 1s electrons. In the case of a complete material transfer, the substrate/stamp ratio of the Ir 4f and F 1s electrons should be comparable to the ratio of the feature/background areas in the fluorescence histogram. XPS table in Fig. 7 shows that the average distribution of the Ir and F atoms in the substrates (44.6% and 43.1%) and stamps (55.4% and 56.9%) correlates well with the ratio of the feature (43%) and background (57%) areas in the fluorescence image of the printed pattern, suggesting complete material transfer.

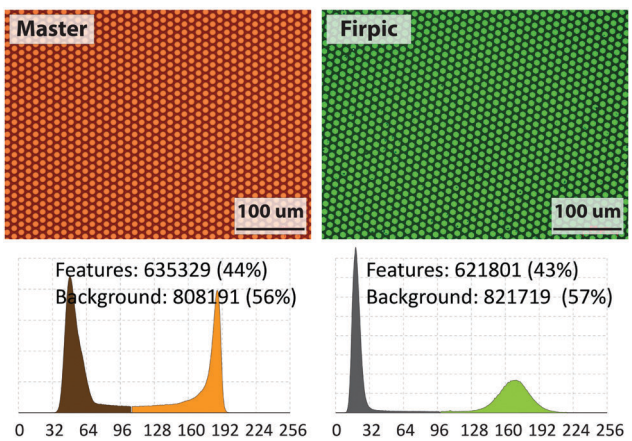

	Sample Name	F 1s	C 1s	Ir 4f	Ir/C	F/C
Features	ITO/TAPC (post-print) 1	94.7088	28993.27	30.86547	0.001065	0.003267
	ITO/TAPC (post-print) 2	105.921	30766.35	40.14892	0.001305	0.003443
	ITO/TAPC (post-print) 3	158.6569	31358.69	29.71583	0.000948	0.005059
	ITO/TAPC (post-print) 4	133.6388	30626.8	30.59856	0.000999	0.004363
				Average	*0.001079*	*0.004033*
				Percentage	*44.6%*	*43.1%*
Background	PUA Stamp (post-print) 1	133.1309	28251.31	52.06906	0.001843	0.004712
	PUA Stamp (post-print) 2	170.0767	29940.32	52.62446	0.001758	0.005681
	PUA Stamp (post-print) 3	158.3993	26836.79	29.56331	0.001102	0.005902
	PUA Stamp (post-print) 4	131.553	26277.41	17.31655	0.000659	0.005006
				Average	*0.00134*	*0.005325*
				Percentage	*55.4%*	*56.9%*

Fig. 7 Top micrographs and histograms: optical images and monochromatic histograms of the original silicon master and the fluorescence pattern; bottom table: XPS analysis of the TAPC-covered ITO substrate and the TCTA/Firpic-covered PUA stamp after the contact transfer.

Sub-micrometer patterns of thin films

Together, our printing experiments show that when a substantial surface energy mismatch exists between the thin film and the printing stamp, uniform, accurate and complete material transfer is possible without the kinetic modulation of the viscoelastic stamp properties. This opens up a possibility for the accurate replication of sub-micrometer features – a task complicated in the kinetic modulation by the inverse proportionality of the interfacial energy release rate (G) to the feature diameter, and the resulting weakening dependence of G on the printing velocity with the decrease in the feature size. To show that our method can pattern small sub-micrometer patterns, we used polycarbonate CD molds bearing periodic patterns of 500 nm lines separated by 1000 nm groves to create **PUA** stamps with sub-micrometer features (Fig. 8). These stamps were used to pattern 1000 nm TCTA/Firpic lines (separated by 500 nm) on TAPC/ITO substrates. We discovered that the optimal printing temperature for this sub-micrometer printing was lower than the temperature required to achieve uniform replication of micrometer objects (60 °C *vs.* 80 °C). This suggests that the higher polymer storage modulus is required to enable accurate replication of sub-micrometer patterns. Patterns printed at higher

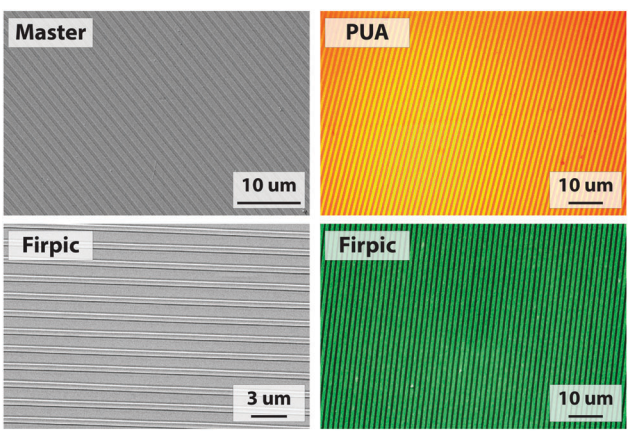

Fig. 8 Top left: SEM image of the sub-micrometer patterns on polycarbonate CD; top right: optical image of the duplicated patterns on PUA stamps; SEM (bottom left) and fluorescence (bottom right) images of the patterned TCTA/Firpic lines on the TAPC-covered ITO.

temperatures (65 and 80 °C) contained numerous defects and were incomplete. Fluorescence and SEM (Au metallized) images of the printed patterns show accurate and uniform features with dimensions similar to the dimension of the features in the original master. To the extent of our knowledge, this is the first demonstration of the sub-micrometer pattern of electroluminescent materials printed on top of the organic semiconductors prepared with a polymeric stamp.

OLED devices with printed emitting layers

The efficiency of the pattern replication that relies on the mechanical delamination and adhesive transfer of organic films is determined not only by the uniformity and geometrical characteristic of the printed features, but also by the nature and proximity of the created interface between the receiving substrate and the thin film. The properties of this contact are especially important in electronics, where the device efficiency directly depends on the uniform and conformal adhesion of material layers. To examine the nature of the contact between the printed emitting features and the continuous TCTA layer, we used the printed substrates to manufacture complete OLED devices (Fig. 9). OLED properties are very sensitive to the presence of non-conformal layer contacts. Such defects can be easily visualized because they appear as non-emitting black areas in the functional devices. We note that it is normal for the devices manufactured in a typical laboratory environment to have a fair amount of such defects even if they are manufactured using the traditional vacuum deposition (Fig. 9, bottom left). These defects are typically caused by the presence of microscopic contaminants (*e.g.*, dust particles) on the electrode surfaces that preclude the formation of continuous conformal layers and by the pin holes in the top electrode layer.

In these experiments, we used previously optimized conditions to patterned features of the green TCTA/Ir(ppy)$_3$ and blue TCTA/Firpic emitting layers on the hole transport TCTA layer. We used two different emitters to show electroluminescence at two different wavelengths (~400 nm Firpic and ~530 nm Ir(ppy)$_3$). To complete the OLED structure, we first deposited 30 nm of the 2,2′,2″-(1,3,5-benzinetriyl)-tris(1-phenyl-1-*H*-benzimidazole) (TPBi) electron transport layer that has an electroluminescence maximum at ~620 nm. This was done to ensure that the Ir(ppy)$_3$ and Firpic electroluminescence could be distinguished from the bulk electroluminescence of the electron transport layer, which is present in the devices with discontinued emitting layers (more typical bathophenanthroline (BPhen) has an electroluminescence maximum that overlaps with the Ir(ppy)$_3$ and Firpic emission). Subsequently, we deposited a 20 nm 1,3,5-tri(*m*-pyridin-3-ylphenyl)benzene (TmPyPB) layer that has a low triplet energy level (2.76 eV) and stops triplet annihilation from the Firpic emitter (2.62 eV triplet energy, see the energy diagram in the ESI†). Finally, we used a 20 nm electron transport BPhen layer to ensure the Ohmic nature of the "device–LiF/Al electrode" contact.

The completed devices were connected to the current–voltage source and examined by optical microscopy and spectrometry. The relevant data of current density, applied voltage and luminance of

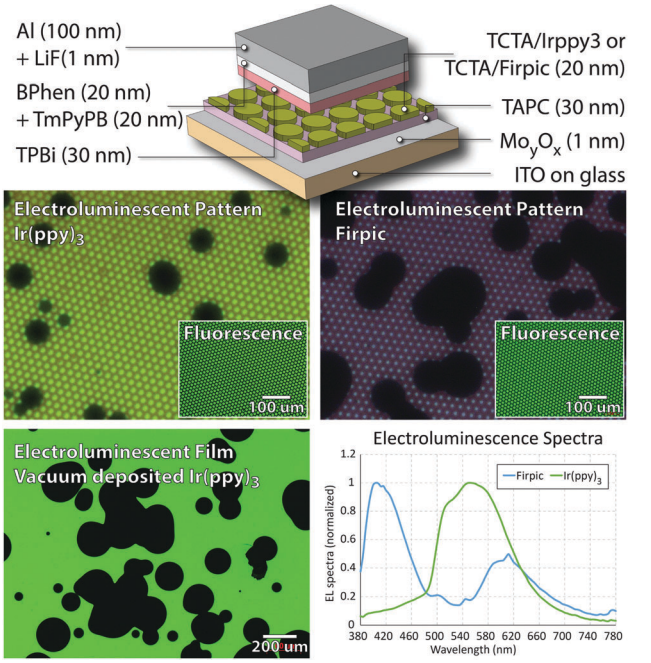

Fig. 9 Top scheme: schematic illustration of the fabricated OLEDs with the patterned green dopant Ir(ppy)$_3$ and the blue dopant Firpic; middle micrographs: optical images of the electroluminescence patterns of corresponding devices with insets of the fluorescence images of the printed Ir(ppy)$_3$ and Firpic layers; bottom left: the electroluminescence optical image of the vacuum-deposited device with a continuous Ir(ppy)$_3$ layer; bottom right: electroluminescence spectra of the OLEDs with printed Ir(ppy)$_3$ and Firpic layers.

the devices were collected. Fig. 9 shows that both devices were functional, containing blue and green electroluminescent dots of the Firpic and Ir(ppy)$_3$ emitters. The electroluminescence spectra of the working devices contain expected maxima at 400 nm (Firpic) and 530 nm (Ir(ppy)$_3$) in addition to the expected emission of TPBi at ~600 nm. The optical micrographs of both devices also demonstrate a reddish background color, suggesting that the TPBi electroluminescence originates from the areas between the features.

The fluorescence patterns show that the printed pixels are uniformly distributed throughout the entire substrate area and that they are accurately replicated without noticeable defects (imaged in at least three different locations). However, the electroluminescence patterns of the completed OLEDs demonstrate a large number of continuous black non-emitting areas, suggesting that the nature of the ITO–TAPC–TCTA/emitter contacts is not uniformly conformal (not shown in Fig. 9). We also observed these defects in the continuous vacuum-deposited device of the similar structure (Fig. 9, bottom left). However, the ratio of the black areas to the emitting regions was significantly higher in the printed devices than in the vacuum-deposited OLEDs. This observation suggests that PUA printing creates less uniform interfaces than vacuum deposition, and that additional optimization of printing conditions or post-printing annealing is needed to improve the contact uniformity.

We then examined if the post-processing annealing at elevated temperatures can increase the area of the conformal contacts.

This journal is © The Royal Society of Chemistry 2016

	Actual Current Density (mA/cm^2)	Drive Voltage (VDC)	Radiance (W-Light/ Sr/m2)	Luminance (cd/m2)	Luminous Yield (cd/A)	1931 CIE x	1931 CIE y	Peak Wave-length (nm)	External Quantum Efficiency (p/e %)
No annealing	5	6.84	2.33	1138	22.8	0.3217	0.6158	517	6.48
80 °C	5	9.16	2.35	1134	22.7	0.2948	0.6287	513	6.47
100 °C	5	6.86	3.11	1502	30	0.2957	0.629	513	8.56
120 °C	5	9.18	0.404	179	3.59	0.3662	0.5489	510	1.14
Vacuum deposition	5	7.07	5.52	2751	55	0.3419	0.6083	521	15.5

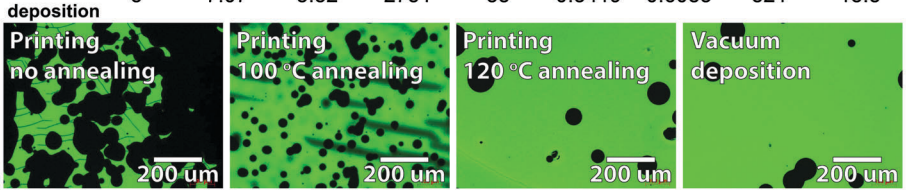

Fig. 10 Top table: measured properties of the OLED devices printed with flat PUA stamps and annealed at various temperatures (23, 80, 100 or 120 °C) and the OLED prepared *via* vacuum deposition without annealing; bottom: electroluminescence micrographs of the devices prepared without annealing, annealed at 100 and 120 °C, and the vacuum-deposited OLED (in this order from left to right).

In these experiments we used flat PUA stamps to deposit continuous TCTA/$Ir(ppy)_3$ layers on TAPC. Subsequently, these layers were annealed at 80, 100 and 120 °C under vacuum, and used to complete the OLED devices. Fig. 10 shows the properties and efficiencies of the printed devices, which are compared to the vacuum-deposited device of identical architecture. We note that the number of the non-emitting defects in the devices with continuous printed layers was substantially higher (before the annealing) than the number of these defects in the patterned devices. We attribute this to a more complex delamination/adhesion contact mechanics that governs the efficient transfer of continuous films. Fig. 10 demonstrates that the proportion of the defect areas decreased with annealing, reaching levels of vacuum-deposited devices (annealing at 120 °C). However, high temperature annealing at 120 °C caused a decrease in the device performance. Devices annealed at 100 °C demonstrated a significantly reduced defect number and an increase in the external quantum efficiency. These results serve as a promising starting point for the future studies targeted to improve the efficiency of PUA contact printing for electronic applications.

Conclusions

This study shows that PUA-based polymers can be used in a broad array of contact printing applications enabling the patterning of different molecular and multilayered thin films. A unique feature of our method is that the separation and transfer of the printed materials are controlled almost entirely by the tunable surface energy of the PUA stamps, without relying on additional releasing layers or stamping kinetics to modulate the adhesion. As a result, our method offers a simplified and uniform set of printing conditions that can be easily adapted to print various materials. To support these claims, we have demonstrated that PUA stamps can be used in the diffusive microcontact printing of various organic monolayers and in the patterning of semiconducting organic thin films. We showed that PUA-based printing yields accurate and uniform patterns and that it does not degrade the printed materials. We have also demonstrated that the PUA-based contact printing can be used to produce sub-micrometer patterns of organic thin films – a challenging task for PDMS-based printing that relies on the modulation of stamping kinetics.

Acknowledgements

Financial support of NSF (ECCS 1530540 and DMR 1228889) is gratefully acknowledged. We thank Prof. Ching W. Tang and Prof. Mitchell Anthamatten for their invaluable help in this study and in the preparation of this manuscript.

Notes and references

1 A. Kumar and G. M. Whitesides, *Appl. Phys. Lett.*, 1993, **63**, 2002–2004.
2 B. Michel, A. Bernard, A. Bietsch, E. Delamarche, M. Geissler, D. Juncker, H. Kind, J.-P. Renault, H. Rothuizen, H. Schmid, P. Schmidt-Winkel, R. Stutz and H. Wolf, *IBM J. Res. Dev.*, 2001, **45**, 697–719.
3 A. Perl, D. N. Reinhoudt and J. Huskens, *Adv. Mater.*, 2009, **21**, 2257–2268.
4 J. A. Rogers and R. G. Nuzzo, *Mater. Today*, 2005, **8**, 50–56.
5 R. K. Smith, P. A. Lewis and P. S. Weiss, *Prog. Surf. Sci.*, 2004, **75**, 1–68.
6 D. B. Weibel, W. R. DiLuzio and G. M. Whitesides, *Nat. Rev. Microbiol.*, 2007, **5**, 209–218.
7 Y. Xia and G. M. Whitesides, *Angew. Chem., Int. Ed.*, 1998, **37**, 550–575.
8 J. T. Koepsel and W. L. Murphy, *ChemBioChem*, 2012, **13**, 1717–1724.
9 T. Kaufmann and B. J. Ravoo, *Polym. Chem.*, 2010, **1**, 371–387.
10 M. Mrksich, *Acta Biomater.*, 2009, **5**, 832–841.

11 A. B. Braunschweig, F. Huo and C. A. Mirkin, *Nat. Chem.*, 2009, **1**, 353–358.
12 S. A. Ruiz and C. S. Chen, *Soft Matter*, 2007, **3**, 168–177.
13 P. M. Mendes, C. L. Yeung and J. A. Preece, *Nanoscale Res. Lett.*, 2007, **2**, 373–384.
14 J. C. Love, L. A. Estroff, J. K. Kriebel, R. G. Nuzzo and G. M. Whitesides, *Chem. Rev.*, 2005, **105**, 1103–1169.
15 D.-H. Kim, N. Lu, R. Ma, Y.-S. Kim, R.-H. Kim, S. Wang, J. Wu, S. M. Won, H. Tao, A. Islam, K. J. Yu, T.-i. Kim, R. Chowdhury, M. Ying, L. Xu, M. Li, H.-J. Chung, H. Keum, M. McCormick, P. Liu, Y.-W. Zhang, F. G. Omenetto, Y. Huang, T. Coleman and J. A. Rogers, *Science*, 2011, **333**, 838–843.
16 W.-H. Yeo, Y.-S. Kim, J. Lee, A. Ameen, L. Shi, M. Li, S. Wang, R. Ma, S. H. Jin, Z. Kang, Y. Huang and J. A. Rogers, *Adv. Mater.*, 2013, **25**, 2773–2778.
17 A. Takakuwa, *Mol. Electron. Bioelectron.*, 2009, **20**, 111–114.
18 A. Carlson, A. M. Bowen, Y. G. Huang, R. G. Nuzzo and J. A. Rogers, *Adv. Mater.*, 2012, **24**, 5284–5318.
19 D.-H. Kim, R. Ghaffari, N. Lu and J. A. Rogers, *Annu. Rev. Biomed. Eng.*, 2012, **14**, 113–128.
20 J. A. Rogers, T. Someya and Y. Huang, *Science*, 2010, **327**, 1603–1607.
21 M. Su, F. Li, S. Chen, Z. Huang, M. Qin, W. Li, X. Zhang and Y. Song, *Adv. Mater.*, 2016, **28**, 1369–1374.
22 B. Su, C. Zhang, S. Chen, X. Zhang, L. Chen, Y. Wu, Y. Nie, X. Kan, Y. Song and L. Jiang, *Adv. Mater.*, 2014, **26**, 2501–2507.
23 X. M. Li, M. Peter, J. Huskens and D. N. Reinhoudt, *Nano Lett.*, 2003, **3**, 1449–1453.
24 M. J. Owen and P. J. Smith, *J. Adhes. Sci. Technol.*, 1994, **8**, 1063–1075.
25 B. Olander, A. Wirsen and A. C. Albertsson, *J. Appl. Polym. Sci.*, 2004, **91**, 4098–4104.
26 C. Y. Hui, A. Jagota, Y. Y. Lin and E. J. Kramer, *Langmuir*, 2002, **18**, 1394–1407.
27 J. K. Hwang, S. Cho, J. M. Dang, E. B. Kwak, K. Song, J. Moon and M. M. Sung, *Nat. Nanotechnol.*, 2010, **5**, 742–748.
28 J. Yoon, A. J. Baca, S.-I. Park, P. Elvikis, J. B. Geddes, L. Li, R. H. Kim, J. Xiao, S. Wang, T.-H. Kim, M. J. Motala, B. Y. Ahn, E. B. Duoss, J. A. Lewis, R. G. Nuzzo, P. M. Ferreira, Y. Huang, A. Rockett and J. A. Rogers, *Nat. Mater.*, 2008, **7**, 907–915.
29 K. G. Sharp, G. S. Blackman, N. J. Glassmaker, A. Jagota and C. Y. Hui, *Langmuir*, 2004, **20**, 6430–6438.
30 E. Delamarche, H. Schmid, B. Michel and H. Biebuyck, *Adv. Mater.*, 1997, **9**, 741–746.
31 H. A. Biebuyck, N. B. Larsen, E. Delamarche and B. Michel, *IBM J. Res. Dev.*, 1997, **41**, 159–170.
32 S. Choi, P. J. Yoo, S. J. Baek, T. W. Kim and H. H. Lee, *J. Am. Chem. Soc.*, 2004, **126**, 7744–7745.
33 Y. S. Kim, H. H. Lee and P. T. Hammond, *Nanotechnology*, 2003, **14**, 1140–1144.
34 J.-P. Wolf, A. Schulthess, B. Steinmann and M. Hunziker, *EP Pat.*, 94-810110, 614122, 1994.
35 P. J. Yoo, S.-J. Choi, J. H. Kim, D. Suh, S. J. Baek, T. W. Kim and H. H. Lee, *Chem. Mater.*, 2004, **16**, 5000–5005.
36 C. M. Bowers, E. J. Toone, R. L. Clark and A. A. Shestopalov, *J. Visualized Exp.*, 2011, e3478, DOI: 10.3791/3478.
37 C. M. Bowers, M. Zhang, Y. L. Lyubarskaya, C. W. Tang and A. A. Shestopalov, *Adv. Mater. Interfaces*, 2014, **1**, 1–7.
38 A. A. Shestopalov, R. L. Clark and E. J. Toone, *J. Am. Chem. Soc.*, 2007, **129**, 13818–13819.
39 A. A. Shestopalov, R. L. Clark and E. J. Toone, *Nano Lett.*, 2010, **10**, 43–46.
40 A. A. Shestopalov, C. J. Morris, B. N. Vogen, A. Hoertz, R. L. Clark and E. J. Toone, *Langmuir*, 2011, **27**, 6478–6485.
41 M. K. Kwak, T.-i. Kim, P. Kim, H. H. Lee and K. Y. Suh, *Small*, 2009, **5**, 928–932.
42 D.-G. Choi, K.-J. Lee, J.-H. Jeong, D. Hwan Wang, O. Ok Park and J. Hyeok Park, *Sol. Energy Mater. Sol. Cells*, 2013, **109**, 1–7.
43 C. Jun-ho, K. Kyung-Ho, C. Se-Jin and H. L. Hong, *Nanotechnology*, 2006, **17**, 2246.
44 K.-H. Kim, K.-W. Bong and H. H. Lee, *Appl. Phys. Lett.*, 2007, **90**, 093505.
45 S.-m. Seo, J. H. Kim and H. H. Lee, *Appl. Phys. Lett.*, 2006, **89**, 253515.
46 J. K. Kim, W. Kim, D. H. Wang, H. Lee, S. M. Cho, D.-G. Choi and J. H. Park, *Langmuir*, 2013, **29**, 5377–5382.
47 S. Y. Park, T. Kwon and H. H. Lee, *Adv. Mater.*, 2006, **18**, 1861–1864.
48 C. J. Campbell, S. K. Smoukov, K. J. M. Bishop and B. A. Grzybowski, *Langmuir*, 2005, **21**, 2637–2640.
49 P. W. Snyder, M. S. Johannes, B. N. Vogen, R. L. Clark and E. J. Toone, *J. Org. Chem.*, 2007, **72**, 7459–7461.
50 P. J. Yoo, S.-J. Choi, J. H. Kim, D. Suh, S. J. Baek, T. W. Kim and H. H. Lee, *Chem. Mater.*, 2004, **16**, 5000–5005.
51 K. L. Chopra, S. Major and D. K. Pandya, *Thin Solid Films*, 1983, **102**, 1–46.
52 A. L. Dawar and J. C. Joshi, *J. Mater. Sci.*, 1984, **19**, 1–23.
53 J. Kido, M. Kimura and K. Nagai, *Science*, 1995, **267**, 1332–1334.
54 H. Kim, *Appl. Phys. Lett.*, 1999, **74**, 3444.
55 Y.-H. Tak, K.-B. Kim, H.-G. Park, K.-H. Lee and J.-R. Lee, *Thin Solid Films*, 2002, **411**, 12–16.
56 C. Tang, *Appl. Phys. Lett.*, 1986, **48**, 183.
57 C. W. Tang and S. A. VanSlyke, *Appl. Phys. Lett.*, 1987, **51**, 913–915.
58 A. Berlin, G. Zotti, G. Schiavon and S. Zecchin, *J. Am. Chem. Soc.*, 1998, **120**, 13453–13460.
59 S.-Y. Oh, Y.-J. Yun, D.-Y. Kim and S.-H. Han, *Langmuir*, 1999, **15**, 4690–4692.
60 C. Yan, M. Zharnikov, A. Gölzhäuser and M. Grunze, *Langmuir*, 2000, **16**, 6208–6215.
61 T. Kondo, M. Takechi, Y. Sato and K. Uosaki, *J. Electroanal. Chem.*, 1995, **381**, 203–209.
62 H. Yamada, H. Imahori, Y. Nishimura, I. Yamazaki and S. Fukuzumi, *Chem. Commun.*, 2000, 1921–1922, DOI: 10.1039/B006108P.
63 J. T. Sullivan, K. E. Harrison, J. P. Mizzell and S. M. Kilbey, *Langmuir*, 2000, **16**, 9797–9803.

 This journal is © The Royal Society of Chemistry 2016

64 J. E. Malinsky, G. E. Jabbour, S. E. Shaheen, J. D. Anderson, A. G. Richter, T. J. Marks, N. R. Armstrong, B. Kippelen, P. Dutta and N. Peyghambarian, *Adv. Mater.*, 1999, **11**, 227–231.
65 H. Hillebrandt and M. Tanaka, *J. Phys. Chem. B*, 2001, **105**, 4270–4276.
66 S. F. J. Appleyard, S. R. Day, R. D. Pickford and M. R. Willis, *J. Mater. Chem.*, 2000, **10**, 169–173.
67 C. K. Luscombe, H. W. Li, W. T. S. Huck and A. B. Holmes, *Langmuir*, 2003, **19**, 5273–5278.
68 P. M. StJohn and H. G. Craighead, *J. Vac. Sci. Technol., B: Microelectron. Nanometer Struct.–Process., Meas., Phenom.*, 1996, **14**, 69–74.
69 B. M. Silverman, K. A. Wieghaus and J. Schwartz, *Langmuir*, 2005, **21**, 225–228.
70 I. L. Liakos, R. C. Newman, E. McAlpine and M. R. Alexander, *Surf. Interface Anal.*, 2004, **36**, 347–354.
71 T.-H. Tsai and Y.-F. Wu, *Microelectron. Eng.*, 2006, **83**, 536–541.
72 M. A. Meitl, Z.-T. Zhu, V. Kumar, K. J. Lee, X. Feng, Y. Y. Huang, I. Adesida, R. G. Nuzzo and J. A. Rogers, *Nat. Mater.*, 2006, **5**, 33–38.
73 A. J. Baca, J.-H. Ahn, Y. Sun, M. A. Meitl, E. Menard, H.-S. Kim, W. M. Choi, D.-H. Kim, Y. Huang and J. A. Rogers, *Angew. Chem., Int. Ed.*, 2008, **47**, 5524–5542.
74 Y. Sun, H.-S. Kim, E. Menard, S. Kim, I. Adesida and J. A. Rogers, *Small*, 2006, **2**, 1330–1334.
75 Y. Sun and J. A. Rogers, *Adv. Mater.*, 2007, **19**, 1897–1916.
76 T.-H. Kim, W. M. Choi, D.-H. Kim, M. A. Meitl, E. Menard, H. Jiang, J. A. Carlisle and J. A. Rogers, *Adv. Mater.*, 2008, **20**, 2171–2176.

This journal is © The Royal Society of Chemistry 2016